

*“Nem a kép tárgya a fontos,  
hanem a szellemi valóság, amely általa testet öltött.”*

Bernáth Aurél

# **Exogen and endogen events trigger complex interactions in melanoma microenvironment**

PhD Thesis

Edina Gyukity-Sebestyén

Supervisor:

Krisztina Buzás, PhD

Department of Immunology, Faculty of Medicine, Faculty of Science and Informatics,

University of Szeged

Biological Research Centre, Institute of Biochemistry



Doctoral School of Interdisciplinary Medicine,

Faculty of Medicine, University of Szeged

Szeged

2020

The dissertation is based on the following publications:

- I. **Gyukity-Sebestyén E**, Harmati M, Dobra G, Németh IB, Mihály J, Zvara Á, Hunyadi-Gulyás É, Katona R, Nagy I, Horváth P, Bálint Á, Szkalicity Á, Kovács M, Pankotai T, Borsos B, Erdélyi M, Szegletes Z, Veréb ZJ, Buzás EI, Kemény L, Bíró T, Buzás K. Melanoma-Derived Exosomes Induce PD-1 Overexpression and Tumor Progression via Mesenchymal Stem Cell Oncogenic Reprogramming. *Front Immunol.* **10**, 2459. doi: [10.3389/fimmu.2019.02459](https://doi.org/10.3389/fimmu.2019.02459) (2019) **IF 5.085; Q1**
- II. Buzás K, Marton A, Vizler C, **Gyukity-Sebestyén E**, Harmati M, Nagy K, Zvara Á, Katona RL, Tubak V, Endrész V, Németh IB, Oláh J, Vigh L, Bíró T, Kemény L. Bacterial Sepsis Increases Survival in Metastatic Melanoma: Chlamydomonas Pneumoniae Induces Macrophage Polarization and Tumor Regression. *J Invest Dermatol.* **136**, 862-5. doi: [10.1016/j.jid.2015.12.032](https://doi.org/10.1016/j.jid.2015.12.032) (2016) **IF 6.287; Q1**

Further publications:

- I. Dobra G, Bukva M, Szabo Z, Bruszel B, Harmati M, **Gyukity-Sebestyén E**, Jenei A, Szucs M, Horvath P, Biro T, Klekner A, Buzas K. Small Extracellular Vesicles Isolated from Serum May Serve as Signal-Enhancers for the Monitoring of CNS Tumors. *Int J Mol Sci.* **21**(15). doi: [10.3390/ijms21155359](https://doi.org/10.3390/ijms21155359) (2020) **IF 4.556; Q2**
- II. Harmati M, **Gyukity-Sebestyén E**, Dobra G, Janovak L, Dekany I, Saydam O, Hunyadi-Gulyas E, Nagy I, Farkas A, Pankotai T, Ujfaludi Z, Horvath P, Piccinini F, Kovacs M, Biro T, Buzas K. Small extracellular vesicles convey the stress-induced adaptive responses of melanoma cells. *Sci Rep.* **9**;15329. doi: [10.1038/s41598-019-51778-6](https://doi.org/10.1038/s41598-019-51778-6) (2019) **IF 3.998; Q1**
- III. Zsedenyi A, Farkas B, Abdelrasoul GN, Romano I, **Gyukity-Sebestyén E**, Nagy K, Harmati M, Dobra G, Korondi S, Decsi G, Nemeth IB, Diaspro A, Brandi F, Beke S, Buzas K. Gold nanoparticle-filled biodegradable photopolymer scaffolds induced muscle remodeling: *in vitro* and *in vivo* findings. *Mater Sci Eng C Mater Biol Appl.* **72**,625-630. doi: [10.1016/j.msec.2016.11.124](https://doi.org/10.1016/j.msec.2016.11.124) (2016) **IF 5.08; Q1**
- IV. Harmati M, Tarnai Z, Decsi G, Korondi S, Szegletes Z, Janovak L, Dekany I, Saydam O, **Gyukity-Sebestyén E**, Dobra G, Nagy I, Nagy K, Buzas K. Stressors alter intercellular communication and exosome profile of nasopharyngeal carcinoma cells. *J Oral Pathol Med.* **46**,259-266. doi: [10.1111/jop.12486](https://doi.org/10.1111/jop.12486) (2017) **IF 2.237; Q2**
- V. Harmati M, **Gyukity-Sebestyén E**, Dobra G, Terhes G, Urban E, Decsi G, Mimica-Dukić N, Lesjak M, Simin N, Pap B, Nemeth IB, Buzas K. Binary mixture of *Satureja hortensis* and *Origanum vulgare* subsp. *hirtum* essential oils: *in vivo* therapeutic efficiency against *Helicobacter pylori* infection. *Helicobacter.* **22**,e12350. doi: [10.1111/hel.12350](https://doi.org/10.1111/hel.12350) (2017) **IF 4.123; Q1**
- VI. Dobó J, Harmat V, Beinrohr L, **Sebestyén E**, Závodszy P, Gál P. MASP-1, a promiscuous complement protease: structure of its catalytic region reveals the basis of its broad specificity. *J Immunol.* **183**,1207-14. doi: [10.4049/jimmunol.0901141](https://doi.org/10.4049/jimmunol.0901141) (2009) **IF 5.0; Q1**
- VII. Dobó J, Harmat V, **Sebestyén E**, Beinrohr L, Závodszy P, Gál P. Purification, crystallization and preliminary X-ray analysis of human mannose-binding lectin-associated serine protease-1 (MASP-1) catalytic region. *Acta Cryst.* **64**,781-784. doi: [10.1107/S174430910802294X](https://doi.org/10.1107/S174430910802294X) (2008) **IF 0.91; Q3**

# 1. Introduction

Hanahan and Weinberg proposed the ten hallmarks of cancer, which provided a useful conceptual structure for understanding the complex biology of cancer (Fig. 1).

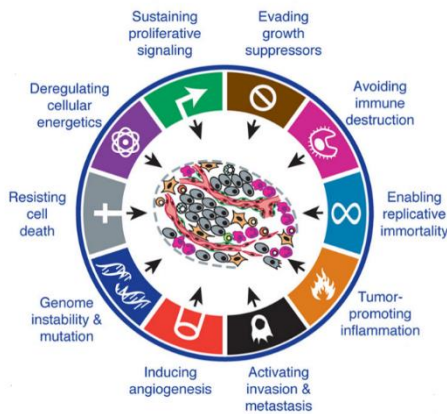


Figure 1. The hallmarks of cancer.

The tumor mass consists not only of a heterogeneous population of cancer cells but also a variety of resident and infiltrating host cells, secreted factors, and extracellular matrix proteins, known as the tumor microenvironment (TME). The TME is a dynamic milieu, which is continuously evolving. Cancer cells manipulate their microenvironment through the secretion of various cytokines, chemokines, growth factors and extracellular vesicles (EVs). The development of a supporting niche is critical for the continuous and uncontrolled growth of cancer.

Mesenchymal stem cells (MSCs) are a major component of the TME. The MSCs home to a cancer microenvironment in response to various cytokines, chemokines and EVs secreted by cancer cells. Under tumoral influence, MSCs have been shown to differentiate into multiple tumor-associated cells types. Conflicting data and concepts about on antitumor and tumor-promoting roles of MSCs have been reported. Indeed, cellular fate could depend on the cancer type and also on the status of the affected MSCs.

Recruitment of monocytes is one of the primary events in tumor development. The phenotype of tumor-associated-macrophage (TAM) is strongly influenced by microenvironmental factors present within the developing tumor. TAMs play a key role in oncogenic processes as tumor proliferation, angiogenesis and metastasis. Mirroring the paradigm of Th1/Th2 lymphocytes, macrophages can be subdivided into two polarized subsets; classically activated macrophages and alternatively activated macrophages, M1 and M2, respectively. M1 cells produce molecules associated with microbicidal and tumoricidal activity. M1 infiltration in tumors is associated with a good prognosis in some cancers. M2 macrophages lose their antigen presenting capabilities and are involved in tissue remodeling, debris scavenging and immune modulation, support angiogenesis, and express immunosuppressive molecules. TAMs can be used as a target for cancer treatment, reducing the number of TAMs or polarizing them towards an M1 phenotype can help destroy cancer cells or impair tumor growth. It has been recognized for over

100 years ago that cancer patients might recover following bacterial infections (Coley's toxins). Although it is generally accepted that anti-tumor immune effector mechanisms overlap with antibacterial immune responses, the exact anti-tumor mechanism induced by microbes is not yet understood.

Metastasis is the hallmark of cancer that is responsible for the greatest number of cancer-related deaths. Stephen Paget's "seed and soil" hypothesis of metastasis, claims that the distribution of cancers is not random. Tumors can induce the formation of microenvironments in distant organs that are conducive to the survival and outgrowth of tumor cells before their arrival at these sites. These predetermined microenvironments are termed pre-metastatic niches (PMNs).

EVs are lipid bound vesicles secreted by cells into extracellular space. There are three main types of such membrane vesicles: microparticles, microvesicles (100–1000 nm), and exosomes (20–200 nm).

The smallest EVs are exosomes (<200 nm), which are formed within the endosomal network through inward budding of MVBs. During this process, numerous proteins, nucleic acid, transcriptional factors, and lipids can be selectively packed into MVB in a cell type-dependent manner. These exosomal-molecular patterns, as unique entities of the complex intercellular communication, are not independent of the quality or state of the mother cell. Indeed, exosomes are claimed to be capable of carrying and conveying tumor-related information and might have a significant role in formation of the tumor microenvironment.

As mentioned above, before metastasis, the target organs are specifically modified to establish a microenvironment suitable for tumor cell growth, known as the PMN. In recent years, EVs have been shown to play a critical role in mediating the interaction between tumor cells and host cells, which prepares the PMN for the formation of secondary sites.

Melanoma is a highly invasive, metastatic cancer with poor prognosis and survival rate. The incidence and mortality rates of cutaneous melanoma differ widely across the globe depending on access to early detection and primary care. In 2018, the age standardized (world standard population) incidence was 12.6 per 100,000 person-year in the EU. A melanoma develops through malignant transformation of melanocytes. These pathogenic events may result from the complex interaction between exogenous and endogenous triggers as well as tumor-intrinsic and immune-related factors. Similarly, to other cancers, melanoma development and progression follows a sequential genetic model that results in activation of oncogenes or inactivation of tumor-suppressor genes. At the protein level, some genetics alteration leads to a reciprocal overstimulation of the affected cellular pathways, mainly the mitogen-activated protein kinase

(MAPK) pathway, the phosphoinositide 3-kinase (PI3K), protein kinase B (AKT), phosphatase and tensine homologue (PTEN), and mammalian target of rapamycin (mTOR) pathway. Melanoma cells are able to escape the immune system, and modify the immune response in order to survive; for example, by reinforcing immune checkpoints.

The PD-1 expression is not a default property of melanoma cells. Of further importance, one paper recently demonstrated that PD-1 overexpressing melanoma cell subpopulations are especially aggressive, and that melanoma PD-1:PD-L1 interactions modulate mTOR signaling, whereby they interfere with programmed cell death. This work addressed the consequences of PD-1 overexpression and experimental inhibition of PD-1 functions (using Pdc1-shRNA or anti-PD-1 antibody). However, it failed to define the factors whose activation of which lead to the generation of PD-1 overexpressing subpopulations. This question, though, especially intriguing, if one considers that one of the most effective immunotherapies available today is based on the blockade of the PD-1:PD-L1 interaction mentioned above.

In addition to genetic changes in melanocytes another, the interaction between the elements of the microenvironment is also a key part of melanoma formation.

## 2. Aims

In this study, we aimed to investigate how TME factors promote the pro-metastatic characteristics of melanoma. Pro-metastatic characteristics often depend on the specific tissue microenvironment. The TME was investigated from two different points of view – from the aspect of tumor, and from the behavior of tumor-infiltrating immune cells.

We aimed to investigate how tumor progression is influenced on the one hand by the tumor-derived exosomes, and, on the other hand, by the various types of tumor-infiltrating macrophages (M1, M2).

We hypothesized that the tumor-derived exosomes promote tumor progression, whereas the M1 polarization of tumor-associated macrophages induces tumor regression.

In this project, we addressed four specific aims:

1. Investigate the cellular and molecular signals of melanoma-derived exosome-induced, intercellular communication-mediated malignant transformation of MSC cultures
2. Inspect the alteration in the expression of PD-1, a melanoma progression marker and therapeutic target, upon exposure to melanoma-derived exosomes
3. Examine the melanoma-derived exosome-induced tumor progression *in vivo*
4. Evaluate the impact of macrophage polarization on tumor regression

### 3. Materials and methods

#### **Mice**

C57BL/6N and immunodeficient NOD/Scid IL2rg null (NSG) mice were obtained from Charles River Laboratories, Sulzfeld, Germany. Mice were housed in pathogen-free conditions and experiments were performed in accordance with national (1998. XXVIII; 40/2013) and European (2010/63/EU) animal ethics guidelines. The experimental protocols were approved by the Animal Experimentation and Ethics Committee of the BRC-HAS and the Hungarian National Animal Experimentation and Ethics Board (clearance numbers: XVI./03521/2011 and CSI/01/3929-4/2017, XVI./03521/2011 and CSI/01/3929-4/2017).

#### **Cell cultures and cell line**

The B16F1 mouse melanoma cell line (ECACC) cultured in DMEM (Lonza) containing 10% FBS (Euroclone), 0.01% sodium pyruvate, 1% MEM non-essential amino acids, 1% MEM vitamin solution, 2 mM L-glutamine and 1% P/S/A (all from Lonza).

Murine MSCs were isolated from C57BL/6N mice. Abdominal inguinal fat pads were excised, rinsed with RPMI 1640 medium, and mechanically dissociated. The dissociated tissue was resuspended in RPMI 1640 containing 100 µg/ml collagenase (Sigma-Aldrich) and incubated at 37°C for 50 min. Collagenase was neutralized with a growth medium containing 10% FBS. After centrifugation at  $470 \times g$  for 15 min, cell pellets were resuspended and washed in the culture medium. After wash, cells were resuspended in complete MecenCult medium (Stemcell Technologies) and filtered through a 100 µm cell strainer (BD Biosciences) to tissue culture dishes, and cultured at 37°C in 5% CO and 90% humidity. The cells were cultured to 80% confluence before being released with trypsin–EDTA and sub-cultured. The purity of MSC cultures were checked by flow cytometry analysis using the Mouse Multipotent Mesenchymal Stromal Cell Marker Antibody Panel (R&D Systems) according to the manufacturer's instructions.

#### ***Cell cultures for in vitro experiments***

Passage 2 MSCs ( $6 \times 10^4$  cell/ml) were plated in cell culture dishes ( $1.5 \times 10^4/\text{cm}^2$ ). After 24 h incubation, MSC cultures were exposed to B16F1-derived exosomes (40 µg/ml exosomal proteins;  $1.5 \times 10^{11}$  exosomes) at every 24 hours. Samples were exposed to exosomes for 24 h, 48 h, 72 h and 96 h and then harvested in method-competent buffer.

#### ***The mouse model for exosomal treatment***

B16F1 cells were administered intravenously ( $1 \times 10^5$  cell/100 µl) to C57BL/6N mice. One week later, tumor bearing mice were randomized and divided into 3 groups (n=10/group). Mice

were injected intravenously with control buffer (100  $\mu$ l), exosome exposed MSCs ( $1 \times 10^5$  cell/100  $\mu$ l) or exosomes (40  $\mu$ g/100  $\mu$ l) 7, 8, 9, 10, 11 days after the tumor injection. One week after the first MSC administration, 3 animals/group were euthanized, their lungs were removed, photographed and stored at  $-80^\circ\text{C}$  for further protein, mRNA and histological analysis. The remained mice were observed for 10 more days. At the end point, the animals were euthanized, and the tumor metastases were investigated. Experiments were repeated 3 times.

#### *Tumor Coverage*

The tumor coverage of lungs, was determined by the analysis of acquired images using the ImageJ software. The area of tumors and the healthy regions was measured, and the mean percentage, SD and p values were calculated in Microsoft Excel.

#### *The mouse model for Chlamydia treatment*

B16F1 cells were administered intravenously ( $1 \times 10^5$  cell/100  $\mu$ l) to immunocompetent C57BL/6 or immunodeficient NOD/Scid IL2rg null (NSG) mice. One week after the tumor cell administration, mice were treated with *Chlamydia pneumoniae* (*C. pneumoniae*) strain CWL-029 propagated in Hep2 cells. *C. pneumoniae* and the mock control (processed Hep2 cells) were heat-inactivated at  $90^\circ\text{C}$  for 30 minutes. Mice were mildly sedated with sodium pentobarbital (7.5 mg/ml) and treated intranasally with  $1 \times 10^6$  IFU *C. pneumoniae* 7, 9, 11, 14, and 16 days after tumor implantation. Since the physical conditions of NSG mice deteriorated extremely rapidly, animals were euthanized at day 14 after the third *C. pneumoniae* treatment. The special advantages of this model are: (i) with intravenous injection of melanoma cells, visible lung tumor metastases develop within 7 days after injection without significant spreading into other organs; and (ii) *C. pneumoniae* is a lung-specific intracellular pathogen with a significant invasion rate even to the lung metastases. After the inhalations 3 animals/group were anaesthetized and their lungs were harvested for protein, mRNA and histological analysis. The remaining mice received the treatments and were followed for survival. At the end-point, the animals were euthanized, their lungs were removed and 3 independent persons counted the number of surface metastases in a blind fashion.

For the survival experiments, groups of mice (n=15) were treated as described 5 times after melanoma implantation. Kaplan-Meier survival curves were analyzed by a log-rank statistical test and  $p \leq 0.05$  was regarded as statistically significant. All animal experiments were authorized by the institutional and national animal welfare committees.

## Reagents

A detailed list of antibodies for Western blotting and immunofluorescence staining is given as Table 1.

antibody	clone	dilution		cat. n
rabbit anti-mouse CD63	polyclonal	1:1,000	biorbyt	orb11317
hamster anti-mouse CD81	Eat-2(EAT)	1:100	LifeSpan Biosciences	LS-C106418
rabbit anti-mouse CD9	EPR2949	1:500	LifeSpan Biosciences	LS-C105676
mouse anti-mouse HSP70	C92F3A-5	1:8,000	Enzo Life Sciences	ADI-SPA-81
rat anti-mouse PD-1	RMP1-14	1:1,000	Biologend	114102
rabbit anti-mouse MLANA	polyclonal	1:200	biorbyt	orb247345
rat anti-mouse CD11b	M1/70	1:50	R&D Systems	MLDP5
goat anti-mouse CD80	polyclonal	1:100	R&D Systems	AF740
Alexa Fluor 555 conjugated anti-rabbit	polyclonal	1:500	ThermoFisher Scientific	A-21428
Alexa Fluor 647 conjugated anti-rat	polyclonal	1:100	Jackson	112-605-062
goat anti-rabbit-HRP	polyclonal	1:1,000	R&D Systems	HAF008
goat anti-rat-HRP	polyclonal	1:1,000	R&D Systems	HAF005
goat anti-Hamster-HRP	polyclonal	1:30,000	ThermoFisher	PA1-29626

Nucleus staining was performed using DAPI (Life Technologies)

## Exosome isolation and characterization

Exosomes were isolated from melanoma cell culture supernatant. B16F1 supernatants were harvested, supplemented by complete protease inhibitor cocktail (Roche) and centrifuged at  $780 \times g$  for 5 min at  $4^{\circ}\text{C}$  to remove intact cells. Then, the supernatants were centrifuged at  $3,900 \times g$  for 15 min at  $4^{\circ}\text{C}$  and filtered through a  $0.2 \mu\text{m}$  membrane (Millipore) to remove larger cell fragments and microvesicles. Exosomes were pelleted by ultracentrifugation at  $150,000 \times g$  (T-1270 rotor at 40,500 rpm) for 1 h at  $4^{\circ}\text{C}$ . The pellet was washed twice and resuspended in DPBS and stored at  $-80^{\circ}\text{C}$ . The concentration of exosomal proteins was determined using a Pierce BCA Protein assay kit (ThermoFisher). Exosomal markers were detected in the resuspended pellet by Western blot analysis. Exosomes were visualized by atomic force microscopy (AFM) as described previously, and scanning electron microscopy (SEM) using 7 nm gold coating (QUORUM Q150) and a field-emission scanning electron microscope (JEOL JSM-7100F/LV).

## Identification of exosomal proteins by mass spectrometry

Exosomal proteins ( $24 \mu\text{g}$ ) were separated in SDS-PAGE. The lanes were each cut into 12-12 equal bands and subjected to in-gel digestion. Tryptic digests of samples were analyzed by LC-MSMS analysis, on an LTQ-Orbitrap Elite (ThermoFisher) mass spectrometer on-line coupled with a nanoHPLC (nanoAcquity, Waters) system, using a data dependent analysis.

Data analysis: searchable peaklists (mgf format) were extracted using ProteomeDiscoverer (ver: 1.4 ThermoFisher) and subjected to database search on our in-house ProteinProspector (ver: 5.14.1) search engine against the *Mus musculus* and *Bos taurus* protein sequences of the Uniprot (UniProtKB.06.11.2014) database completed with human keratins and pig trypsin, altogether 106,330 protein sequences were searched. FDR values were less than 1% in all cases.

For the functional validation, the obtained resulted protein list was analyzed by the “Core Analysis” function included in Ingenuity Pathway Analysis (IPA) software.

### ***Isolation and detection of miRNAs***

Exosomal miRNA sequencing was performed using SOLiD Total RNA-Seq lit for Small RNA Libraries (Applied Biosystems now part of ThermoFisher) according to the manufacturer’s instructions. Raw data quality assessment, read trimming, read mapping and miRNA expression profiling was carried out in CLC Genomics Workbench tool (ver: 8.0.2 CLC Bio now part of Qiagen) using annotated *Mus musculus* miRNA sequences according to the miRBase release 21 as a mapping reference.

### ***Western blot analysis***

Protein samples were resuspended in 4x sample buffer (NuPAGE®, ThermoFisher) and the electrophoresis was performed using 4-12% Bis-Tris Gels (ThermoFisher), and electroblotted onto PVDF membranes (Merck). Proteins were detected using an ECL Plus Western Blotting detection system (Advansta). Immunoreactive signals were detected by using LI-COR ODYSSEY® Fc (Dual-mode imaging system) imager followed by analysis with Odyssey v1.2. Exosomal markers identified by western blot analysis, applied antibodies listed in Tables 1.

### **Cytokine and Chemokine Detection by Proteome Profiling**

Lung samples were lysed in NP40 cell lysis buffer (Thermo Fisher Scientific) and protein content was measured by the Pierce BCA Protein Assay kit (Thermo Fisher Scientific). Expression levels of different cytokines in pooled lung specimens were determined using Mouse Cytokine Array Panel A (R&D Systems), according to the manufacturer’s instructions. Immunoreactive signals were detected by using LI-COR ODYSSEY® Fc (Dual-mode imaging system) imager followed by analysis with Image Studio Lite v5.2.

### **Quantitative reverse transcription PCR (qRT-PCR)**

#### ***Mlana and Mitf qRT-PCR***

Total RNA was purified using the Quick-RNA MiniPrep isolation kit of (Zymo Research). One µg of total RNA was reverse transcribed with random primers using the High-Capacity

cDNA Archive Kit (Applied Biosystems). QRT-PCR were done with FastStart SYBR Green Master mix (Roche) at a final primer concentration of 250 nM.

Relative expression ratios were calculated as normalized ratios to MmRpl27 (Mus musculus ribosomal protein L27) gene. The final relative gene expression ratios were calculated as  $\Delta\Delta Ct$  values.

#### ***TaqMan panel of 40 oncogenes***

RNA was isolated from MSC cells with Qiagen RNeasy Mini Kit, and cDNAs were synthesized with TaqMan Reverse Transcription Reagents. From lungs tissue total RNA was isolated using TRIzol (ThermoFisher), and transcribed into cDNA using the High Capacity cDNA Kit (ThermoFisher). Eighty ng cDNA and TaqMan Gene Expression Master Mix (ThermoFisher) were used for the qPCR experiment. Expression of the examined 44 genes was calculated by  $\Delta\Delta Ct$  method and normalized to the average Ct values of 4 internal controls (PPIA, 18S RNA, ACTB and GAPDH).

For relationship discovery Hierarchical Cluster Analysis was performed by R software. In detail, the “bottom up” agglomerative hierarchical clustering strategy was used, and the results were represented in a tree-based dendrogram. (R software: R. D. C. Team, R: A Language and Environment for Statistical Computing, R Foundation for Statistical Computing, Vienna, Austria, 2008).

#### ***Cytokines and chemokines qRT-PCR***

Total RNA of lungs was purified using a NucleoSpin RNA II RNA isolation kit; first-strand cDNA was synthesized and qRT-PCR reactions were performed on pooled samples (n=3) on a RotorGene 3000 instrument with gene-specific primers (CCL2, CCL3, CD86, IL-12, IL-6, IL-10, CXCL16, CCL7, CD80, CXCL11, CXCL9, IL-23, TNF- $\alpha$ ), and SYBR Green protocol to monitor gene expression. Each individual Ct value was normalized to the average Ct values of four internal control genes ( $\Delta Ct$  values). The final relative gene expression ratios (fold change) were calculated as comparisons of  $\Delta Ct$  values ( $\Delta\Delta Ct$  values). Non-template control sample was used for each PCR run to check the primer-dimer formation.

#### **Histology, immunohistochemistry**

Lung specimens were fixed in 4% buffered formaldehyde; then routine HE histology as well as standardized immunohistochemistry tissue microarrays were performed used antibodies listed in Table 1.

### **Detection of Y chromosome in tumor metastasis (FISH)**

For fluorescence *in situ* hybridization (FISH), chromosome X and Y control probe (Empire Genomics) was used to verify the presence of the Y chromosome of the transplanted mouse adipose stem cells, according to the manufacturer's instructions.

### **Cell proliferation**

After 72 h incubation, exosome-exposed and control MSC cultures were dissociated with trypsin from the culture surface. Cells were washed in medium and counted in a Bürker chamber and a cell counter (Bio-Rad, TC10 Automated Cell Counter).

### **Detection of apoptosis**

Exosome-exposed MSCs and control cells were treated with 100 ng/ml mouse TNF- $\alpha$  (R&D Systems). After 24 h incubation, cell death was determined by the Annexin V Apoptosis Detection Kit with PI (Biolegend) according to the manufacturer's recommendations. Samples were measured by FACS Calibur flow cytometer (BD Biosciences), data were analyzed by Flowing Software (Cell Imaging Core).

### **PD-1 and MLANA detection by immunofluorescence microscopy**

MSC cultures were fixed with 4% paraformaldehyde, permeabilized and blocked with BSA. The applied antibodies listed in Table 1. Images were obtained by confocal laser scanning microscopy (Olympus) and dSTORM super-resolution microscopy using a custom-made inverted microscope based on a Nikon Eclipse Ti-E frame.

### **Network representation by Ingenuity Pathway Analysis**

According to literature data, we established a protein network from the *in vivo* overexpressed genes in the exosome-related animal groups. A custom graphical representation of this network was generated using the Path Explorer tool of the Ingenuity Pathway Analysis (IPA).

### **Statistical analysis**

All of the data are presented as the mean  $\pm$  SD or SEM and represent a minimum of three independent experiments. Statistical parameters including statistical analysis, statistical significance, and n values are reported in the Figure legends. For *in vivo* experiments n = number of animals. For statistical comparison, we performed two-tailed Student's t-test. A value of  $p \leq 0.05$  was considered significant (represented as \* $p \leq 0.05$ , not significant [n.s.]).

## 4. Results

### Isolated vesicles show exosomal properties

First, we isolated EVs from B16F1 mouse melanoma cells, then characterized them based on *MISEV2018*. Overall, the shape and size, and also the protein composition of the isolated vesicles showed exosomal characteristics (Fig. 2).

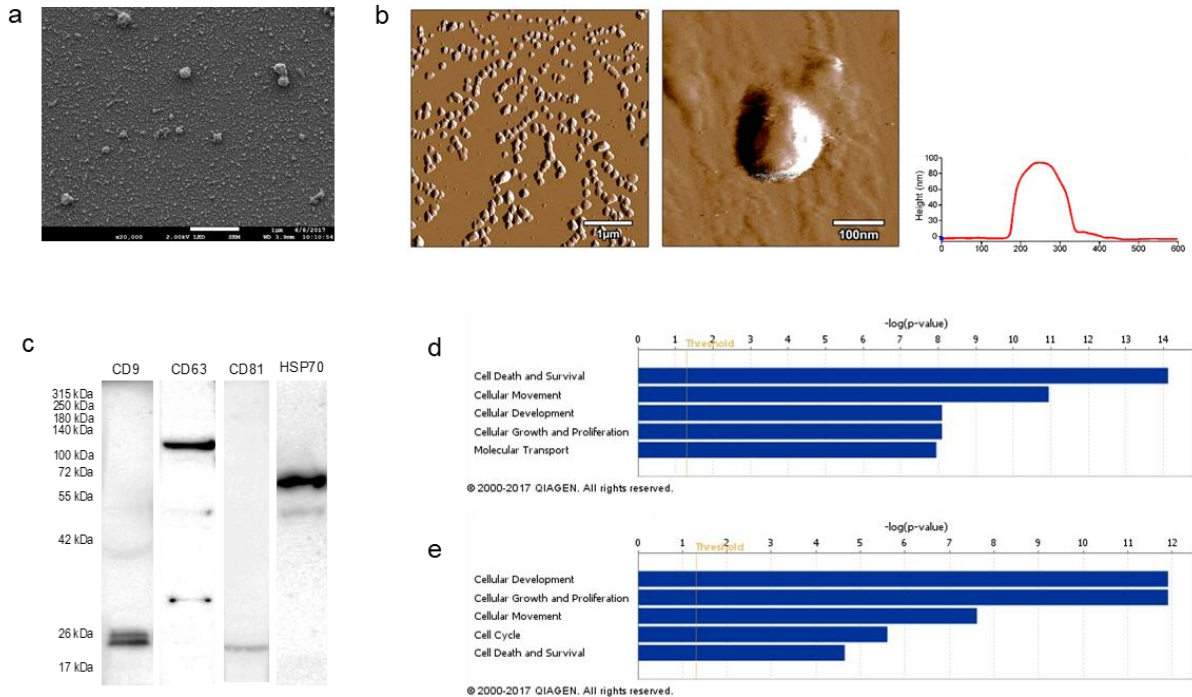


**Figure 2. Characterization of B16F1 melanoma cell culture-derived exosomes.**

(a) SEM of exosomes secreted by melanoma cells. (b) AFM of exosomes. (c) Western blot analysis of common exosome markers. (d and e) The top 5 molecular and cellular functions identified by IPA of exosomal proteins and miRNAs.

Exosomes were then subjected to large-scale analysis to determine their protein and miRNA profiles. Whole proteome analysis revealed that 95 distinct proteins were identified in melanoma exosomes. Further, miRNA sequencing identified 168 known miRNA elements.

To uncover the functional significance of the proteomics and miRNA sequencing data, IPA was employed. This analysis has shown that the identified proteins most probably participated in cellular and molecular processes such as “Cell Death and Survival”, “Cellular Movement”, “Cell-to-Cell Signaling and Interaction”, “Cellular Growth and Proliferation” and “Cell Morphology” (Fig. 2d). Very similarly to these data, functions of the identified miRNAs were suggested to be linked to mechanisms of “Cellular Development”, “Cellular Growth and Proliferation”, “Cellular Movement”, “Cell Cycle” and “Cell Death and Proliferation” (Fig. 2e).

## Tumor exosome exposure resulted in oncogenic reprogramming of MSCs *in vitro*

Then, we investigated the impact of exosomes on the biological processes of MSCs, which are generally considered as adequate *in vitro* models of tumor stroma.

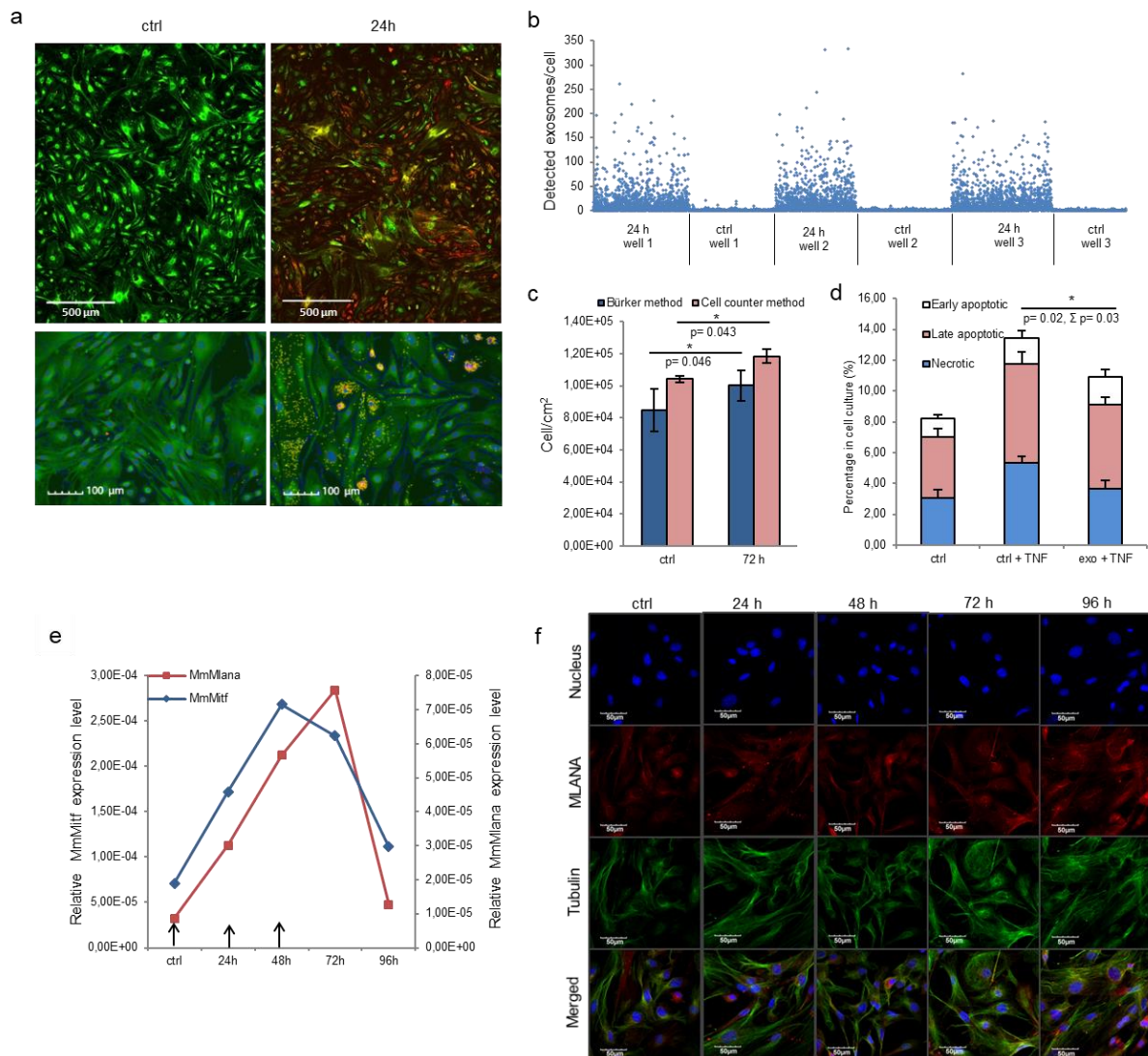


**Figure 3. Internalized melanoma exosomes induce malignant transformation of the recipient MSCs.**

**a)** Cell proliferation assay of exosome-exposed MSCs. Cells were plated in control and exosome-exposed cultures, and 72 h after the exosome treatment, the cell number was showed a significantly increased cell proliferation of exosome-treated cells. Results are presented as mean  $\pm$  SD (n=3). **(b)** Apoptosis analysis of exosome-exposed MSCs by flow cytometry. Both TNF- $\alpha$ -induced total cell death ( $\Sigma$ ) and necrosis were significantly lower ( $\Sigma p=0.03$  and  $p=0.02$ , respectively) in exosome-pretreated cell cultures compared to the corresponding control cells. Results are presented as mean + SD (n=3). **(c)** qRT-PCR analysis of Mlana and Mitf in MSC cultures treated by exosomes in every 24 h as indicated by arrows in the graph. The expression of both mRNAs increased after exosome exposure, but they showed different kinetics. **(d)** Fluorescent immunocytochemistry of MLANA in exosome-exposed MSC cultures using AlexaFluor555-conjugated antibody(red).  $\alpha$ -tubulin network of cells was labeled by an AlexaFluor488-conjugated antibody (green) and the nuclei were stained with DAPI (blue).

We found that proliferation rate of the MSCs significantly accelerated 72 h after exosome exposure (Fig. 3a). Flow cytometry also showed that the exosome-treated MSCs exhibited a partial resistance to the cell death-inducing effects of 100 ng/ml tumor necrosis factor- $\alpha$  (TNF- $\alpha$ ) as the fraction of the dead cells was significantly decreased in these cultures (Fig. 3b).

Since the exosomes were isolated from melanoma cells, we were then intrigued to uncover whether the above alterations also resulted in *de novo* appearance of melanoma-specific features in the transformed MSCs. To answer this question, we assessed the expression of the melanoma-specific markers MLANA and MITF. By qRT-PCR, we found that mRNA transcript levels of both markers elevated markedly in MSCs upon exosome treatment (Fig. 3c). Moreover, immunofluorescence labeling showed that exosome exposure markedly increased the expression of MLANA at the protein level as well (Fig. 3d).

Next, we assessed whether the above effects of exosomes – whereby they induce a malignant-like transformation of the MSCs – was accompanied by a cellular-molecular oncogenic reprogramming of the target cells. Exosome-exposed MSC cultures were subjected to qRT-PCR analysis using a self-designed panel of 40 oncogenes and tumor suppressor genes that were previously suggested to play a role in melanoma progression.

As shown in Fig. 4a, the gene expression pattern of MSCs exposed to melanoma exosomes, exhibited a clear oncogenic dominance (compared to the non-exposed cells). This was verified by statistical analysis of the mean relative gene expression levels of all molecules investigated. Statistically higher values were obtained in the case of exosome-treated cells ( $p = 1.9 \times 10^{-5}$ ,  $p = 0.031$  and  $p = 2.3 \times 10^{-8}$  for the 6 h, 24 h and 72 h time points, respectively).

As mentioned above, one paper has recently shown that melanoma cell subpopulations which overexpress PD-1, quite intriguingly exhibit remarkably increased invasiveness and aggressive growth properties. Since the above finding strongly suggested an “MSC re-education” capacity of melanoma exosomes to induce malignant-like behavior, we next assessed the expression of PD-1 in MSC cultures.

As expected, only insignificant PD-1 expression (both at the mRNA and protein levels) could be identified in control, non-treated MSCs. In contrast, a marked, significant, and time-dependent elevation of PD-1 expression was detected upon exosome treatment by qRT-PCR (Fig. 4b), Western blot and an immunocytochemical analysis (Fig. 4c,d). Furthermore, by employing super-resolution microscopy, we were able to identify a dramatic upregulation of PD-1 at the single molecular level in exosome-treated MSCs (Fig. 4e).

Importantly, since proteomics analysis did not identify the presence of PD-1 in exosomes, these data suggest that the high PD-1 protein content in exosome-exposed MSCs was a result of *de novo* induction and not of exosome-mediated molecular transfer. Our findings therefore suggest that melanoma exosome-mediated “re-education” of the cells resulted in a novel MSC population which could be identified as MSC<sup>PD-1+</sup>.

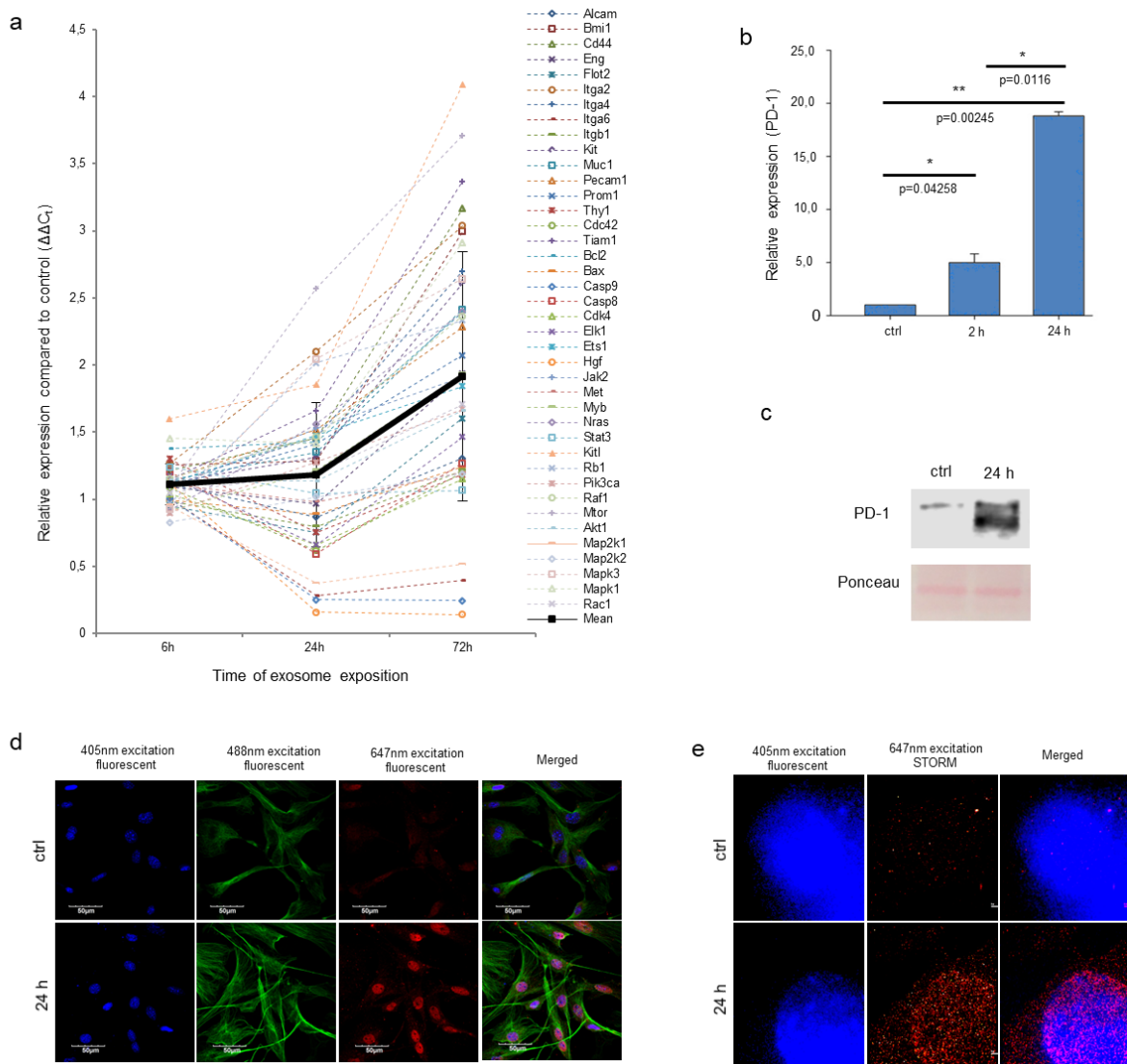


**Figure 4. Exosome re-educated MSCs show oncogene dominance and PD-1 expression.**

(a) qRT-PCR analysis of 40 tumor-related genes in exosome-exposed MSCs using a self-designed panel. The trend line of the altered gene expression pattern shows an increasing tendency over time (mean  $\pm$  SD). (b) qRT-PCR analysis of PD-1 in MSCs after 2 h and 24 h of exosome exposure. The graph represents mean + SEM (n=3). (c) Representative immunoblot of PD-1 protein expression in control and exosome-exposed MSCs after 24 h of exosome treatment. (d,e) Fluorescent immunocytochemistry of PD-1 in 24 h exosome-exposed MSC cultures, using a primary antibody to PD-1 (red). Nuclei were stained with DAPI. (d)  $\alpha$ -tubulin network of cells was labeled green. (e) Images were taken by STORM super-resolution microscopy.

### **B16F1 exosomes augment *in vivo* tumorigenesis and tumor progression**

After presenting evidence for the *in vitro* tumorigenic induction potential of exosomes on cultured MSCs, we hypothesized that this phenomenon could be identified *in vivo* as well. To probe this assumption, we employed the well-known animal model, in which tumors, developed mostly in the lungs, are induced in mice by intravenous administration of mouse B16F1 melanoma cells (to the tail vein). These tumor-bearing mice were then administered by a buffer, or exosomes isolated from the same B16F1 melanoma cells, or exosome-induced MSC<sup>PD-1+</sup> cells.

The exosome-related groups (i.e. groups treated with exosomes or MSC<sup>PD-1+</sup>) were characterized by a markedly increased size of tumor-covered lung tissues (Fig 5a). Of further importance, we also found that in both exosome-related groups, the number of distant metastases were significantly elevated when compared to the control (Fig. 5b). Interestingly, in MSC<sup>PD-1+</sup> treated mice, exosome-transformed MSCs could be identified in the paraaortic lymph nodes by FISH (Fig. 5c) verifying the successful *in vivo* adherence of MSC<sup>PD-1+</sup> cells.

Lung tissues of the different groups were then subjected to in-depth expressional profiling 14 days after injection of exosomes or MSC<sup>PD-1+</sup> cells. Namely, qRT-PCR analysis was performed using a self-designed panel of 40 genes.

Hierarchical cluster analysis (HCA) of the gene expression patterns clearly showed a robust proto-oncogenic dominance in lung samples from the exosome-related groups when compared to the control tissues (Fig. 5d).

Moreover, we showed that, besides the above genes, expression of PD-1 was also significantly increased in both exosome-related groups (Fig. 5e). Notably, although mRNA transcript level of PD-1 was close to two-fold in MSC<sup>PD-1+</sup> lung tissues in comparison to samples in the exosome group, the difference was not significant (most probably due to the large inter-animal variability and standard error).

We constructed a Venn-diagram (Fig. 5f) to show all possible logical connections between the various gene expressions patterns.

Specifically, the following gene expression patterns were defined:

- three genes (Elk1, Rb1, Igta2) were exclusively induced only in the exosome-treated group;
- twenty-three genes (Prom1, Tiam1, Bcl2, Bax, Casp9, Hgf, Jak2, Met, Mapk2k2, Alcam1, Eng, Flot2, Itga4, Itga6, Kit, Pecam1, Thy, Cdc42, Casp8, Ets1, Myb, Map2k1, Mapk1) were found to be upregulated both in the exosome group and the MSC<sup>PD-1+</sup> cell treated groups;
- fourteen genes (Bmi1, Cd44, Itgb1, Muc1, Cdk4, Nras, Sat3, Kitl, Raf1, Mtor, Akt1, Mapk3, Pik3ca, Rac1) were found to be upregulated in all three groups.

Finally, it should be noted that the dramatic gene expression alterations seen in the exosome-related groups were exclusively due to the presence of the exosomes as the “MSC<sup>PD-1+</sup> only” cluster contained no genes (Fig. 5f).

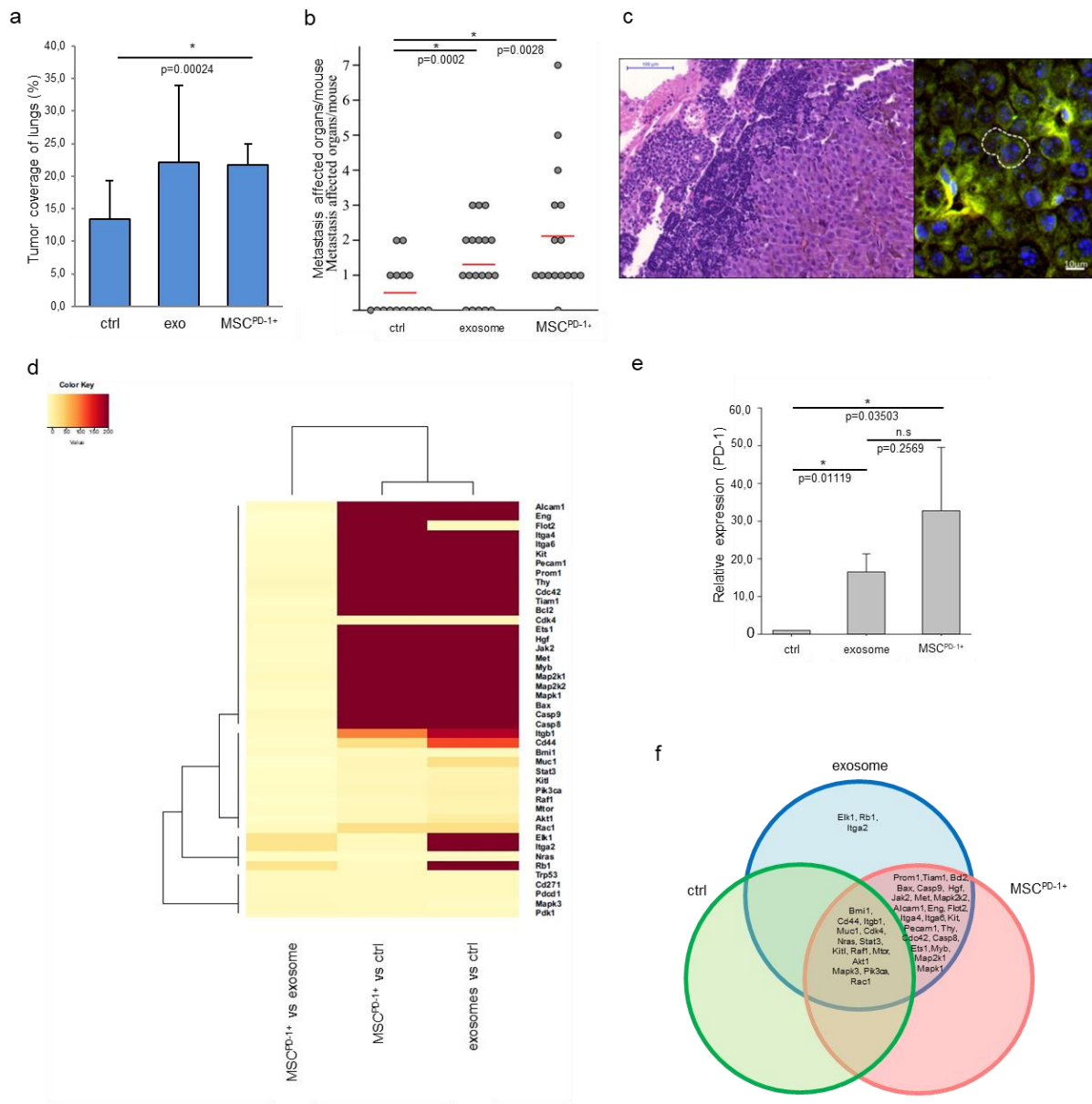


**Figure 5. Melanoma exosomes promote tumor progression and metastasis formation *in vivo*.**

(a) Tumor coverage of lungs on day 15 in the three different animal groups. The graph represents mean + SD (n=3). (b) The number of distant metastases on day 25. One dot represents one animal in each group, red lines show the average number of metastases per animal. (c) FISH analysis of a paraaortic lymph node metastases, which showed the presence of exosome-exposed MSCs. Y chromosome (red dot) of the male mouse-derived MSC was detected in the metastases of a female mouse. (d) Heatmap and cluster analysis of the gene expression pattern, which show protooncogenic dominance in exosome or MSC<sup>PD-1+</sup> groups. (e) qRT-PCR analysis of PD-1 in the lung samples using TaqMan probes (n=3). (f) The Venn diagram shows possible relations between a finite collections of different sets of genes measured during gene expression profiling (see Fig. 5d).

## Melanoma-derived exosomes promote tumorigenic and cell survival signaling pathway(s)

Figure 6 shows the map of interaction pathways based on the overexpressed molecules (red symbols) from the *in vivo* experiments. We detected overexpressed elements from three main pathways which do participate in tumor progression and metastasis formation.

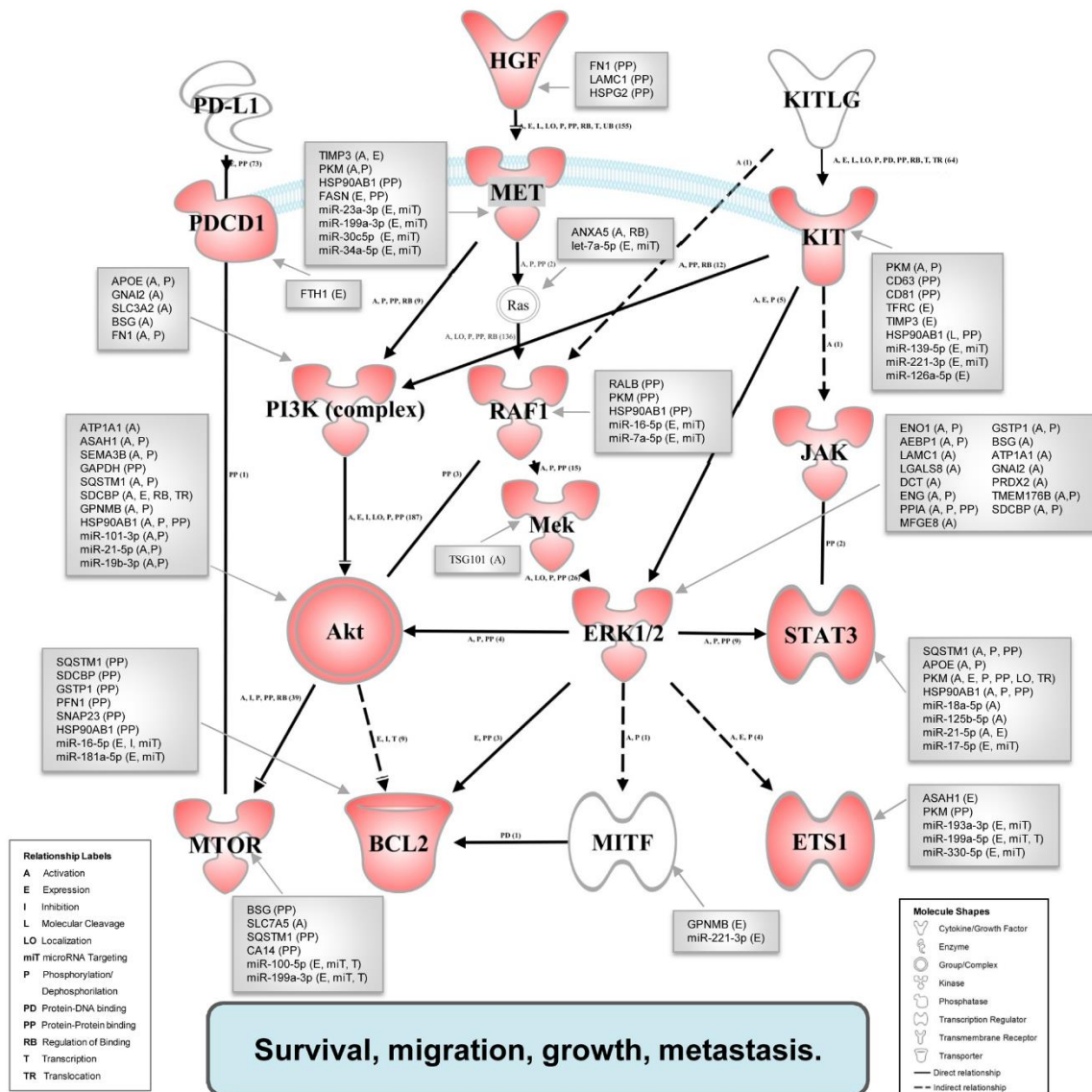


**Figure 6. An integrated associative network of the *in vivo* overexpressed genes supplemented with the interacting exosomal factors.** We created this network of overexpressed genes (red symbols) was conceived by us based on literature data. The relationships between molecules were also supported also by the IPA knowledge base. Network visualization was performed using the Path Explorer tool of the IPA Path Designer. The exosomal proteins and miRNAs (grey boxes) were connected to elements of the network by the Grow tool of the IPA Path Designer based on experimental data of the IPA knowledge base. Activation of the established network by exosomal components may support the survival, migration, growth and metastasis of tumor cells.

Using the IPA Path Designer Grow tool, we generated an interaction map which contains proteins (or their established complexes) encoded by the overexpressed genes, and exosomal

miRNAs and proteins (grey boxes) which were previously shown to control or affect the marked signaling molecules.

These findings demonstrate that the interaction between exosomes and MSCs induces a tumor-like phenotype with PD-1 overexpression of naïve MSCs *in vitro* and a fast tumor progression *in vivo*.

On the other hand, we investigated the melanoma TME on the attitude of tumor-infiltrating immune cells and we demonstrate that bacterial infection may induce a complex anti-tumor immune response.

### **Treatment of immunocompetent mice with *C. pneumoniae* reduces the number of lung metastases and increases survival**

To clarify the role of the tumor associated macrophages in the anti-tumor immune mechanisms induced by *C. pneumoniae*, metastatic melanomas were generated in immunocompetent C57BL/6 mice or immunodeficient NSG mice. B16F1 melanoma cells were administered intravenously to 6 to 8 week old female immunocompetent C57BL/6 or immunodeficient NSG mice. One week after the tumor cell administration, the mice were treated with heat-inactivated *C. pneumoniae* or the mock as a negative control. In immunocompetent animals, the number of lung metastases significantly decreased ( $p = 0.003$ , 3 independent experiments) in the inactivated *C. pneumoniae*-treated group vs. mock (Fig. 7a). Moreover, the survival of the inactivated *C. pneumoniae*-treated mice (Fig. 7b) was significantly increased ( $p = 0.04$ , 3 independent experiments). Importantly, such phenomena were not observed in immunodeficient mice suggesting the anti-tumor role of the immune response.

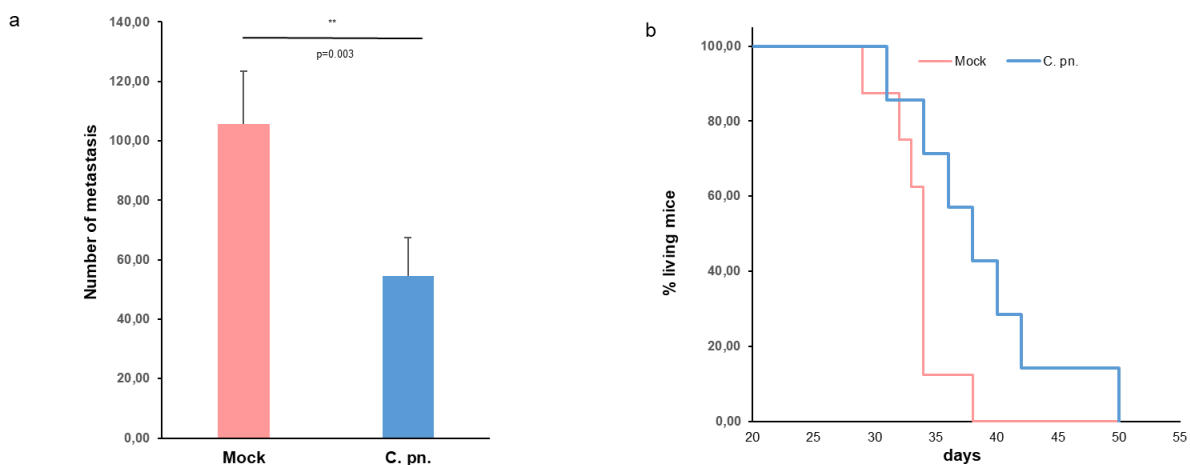


**Figure 7. *C. pneumoniae* treatment results in melanoma metastasis regression and increases survival of animals.** (a) The number of lung metastases and (b) survival rate of mock or *C. pneumoniae* (C. pn.) treated immunocompetent C57BL/6 mice.

### ***C. pneumoniae* treatment induces tumor regression and immune cell infiltration**

Histological sections of lungs from mock-treated melanoma-bearing immunocompetent C57BL/6 mice showed high number of metastases, with frequent intra-tumor necrosis indicating high tumor burden and tumor mass replacing the normal lung tissue (Fig. 8a). In contrast, smaller foci of regressive metastases were observed in the *C. pneumoniae*-treated immunocompetent animals (Fig. 8b). Moreover, in this group, a high number of tumor infiltrating mononuclear histiocytes and lymphoid cells were identified in the regressive metastases compared to mock-treated samples. Notably, in both mock and *C. pneumoniae*-treated immunodeficient NSG mice, the abundant metastases showed mostly subpleural and intraparenchymal localization and no significant intratumor immune reactions (Fig. 8c,d).

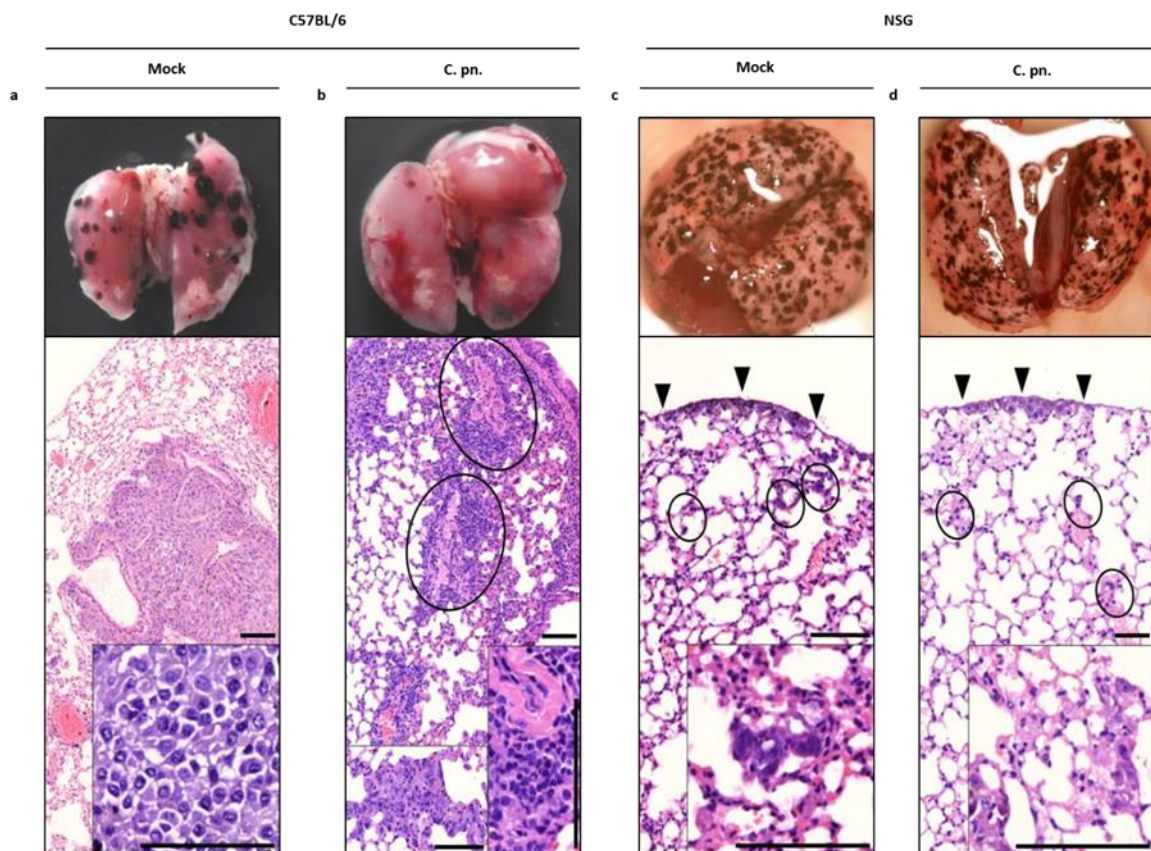


**Figure 8. *C. pneumoniae* treatment induces tumor regression and immune cell infiltration.**

Representative photos and HE-stained histological sections of dissected lungs of mock (a) and *C. pneumoniae* (b) treated immunocompetent mice as well as of mock (c) and *C. pneumoniae* (d) treated immunodeficient (NSG) animals. Scale bars, 100  $\mu$ m. (a) Trophical necroses indicating high tumor burden. Insert: atypical tumor cells and regions of necrosis. (b) Circles and right insert, foci of regressive metastases, left insert: areas of residual pneumonitis after *C. pneumoniae* treatment. (c, d) In both mock and *C. pneumoniae* treated NSG mice, military metastases were developed subpleurally (arrowheads) and intraparenchymally (circles) without significant inflammatory reactions (inserts: higher magnification of intraparenchymal metastases).

The markedly increased immune reaction in the lungs of the *C. pneumoniae*-treated melanoma-bearing C57BL/6 mice was also verified by immunolabeling of cell surface activation markers CD11b and CD80 (Fig. 9). Invasion of immune cells was not detected in the control group

where the immune cells were chiefly concentrated in the marginal zones of the tumors (Fig. 9a,c). However, dramatically increased numbers of tumor-infiltrating, activated (i.e. CD11b and CD80 positive) lymphocytes were detected within the internal tumor stroma of the *C. pneumoniae*-treated animals (Fig. 9b,d); the differences show high levels of significance in both cases (Fig. 9e,f). *C. pneumoniae* treatment induces M1 type macrophage polarization.

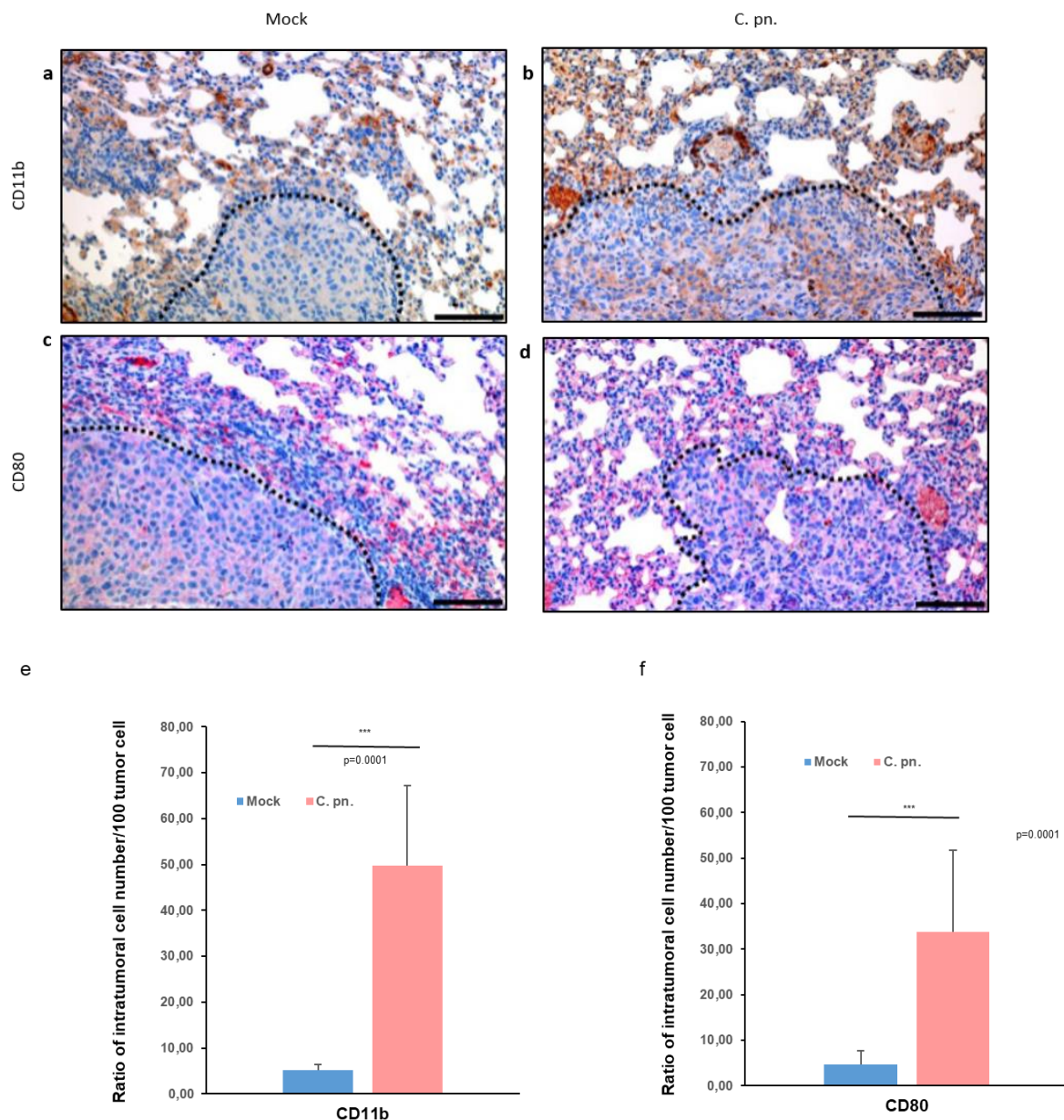


**Figure 9. *C. pneumoniae* treatment results CD11b+ and CD80+ immune cell infiltration of tumor tissues.** Immunohistochemistry of CD11b (a, b, DAB, brown) and CD80 (c, d, Fast red) on lungs of mock (a, c) or *C. pneumoniae* (b, d) treated C57BL/6 mice. Dashed lines indicate tumor border. (a-d). Intratumoral number of CD11b+ (e) and CD80+ (f) cells determined as a ratio of 100 tumor cells. (e, f) Data are expressed as mean + SD.

## The *C. pneumoniae* treatment induces the macrophage differentiation shift toward an M1 phenotype

As a next step, we assessed whether *C. pneumoniae* treatment induced macrophage polarization. To this end, we mapped the cytokine and chemokine transcriptome profiles, characteristics for M1 (anti-tumor) or M2 (pro-tumor) type macrophages, of tumor bearing immunocompetent mice were mapped. M1 and M2 type macrophage markers were detected with qRT-PCR from pooled lung samples (3 animals/pool) 2, 4 and 12 hours after mock or *C. pneumoniae* treatment. qRT-PCR was performed using M1 and M2 type markers. Four hours after *C. pneumoniae* application, markedly increased levels of specific mRNA transcripts for CCL2, CCL3, IL6, CXCL10, CCL7, CD80, CXCL11, CXCL9, IL-23, and TNF- $\alpha$ , markers of M1 type macrophage polarization, were detected (Fig. 10a). In line with these data, mRNA expression of CD163, CCL1, TGF- $\beta$ , and IL-10 (known M2 type macrophage markers) was decreased by the treatment; yet, levels of other important M2 markers (CXCL13, IL-1Ra) were increased (Fig. 10b). Significantly, statistical analysis revealed that upon *C. pneumoniae* administration, the amount of M1 type cytokine and chemokine-specific mRNA transcripts significantly increased ( $p = 0.014$ ) (Fig. 10a) after 4 hours in comparison to M2 type macrophage markers (Fig. 10b).

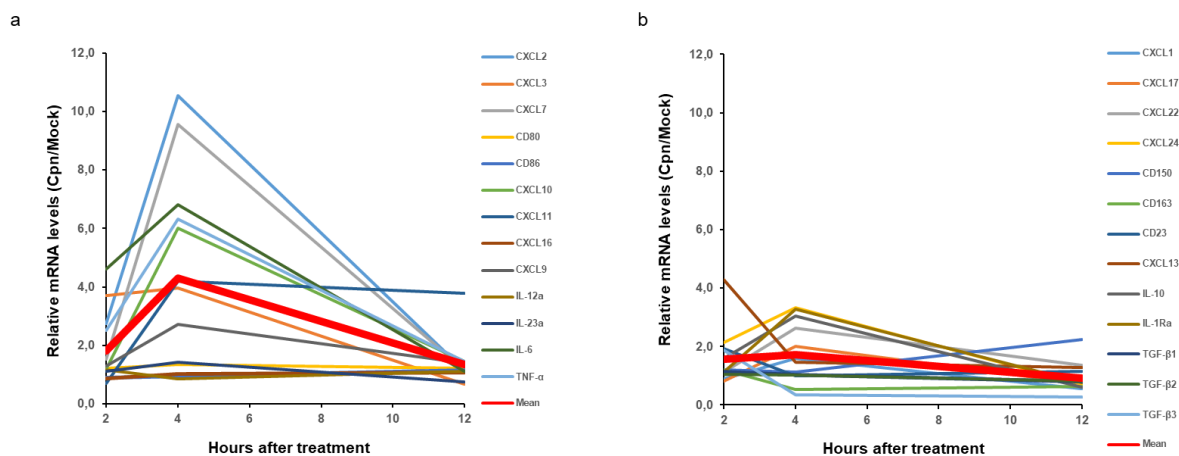


**Figure 10. *C. pneumoniae* treatment induces M1 type macrophage polarization.**

(a) Relative alterations in the levels of individual M1 type cytokine/chemokine specific mRNA transcripts in lung samples of *C. pneumoniae* (*C. pn.*) vs. mock-treated tumor-bearing C57BL/6 mice, as determined by real-time PCR. (b) Mean values of relative M2 cytokine mRNA expressions; at 4 hours after treatment, M1 and M2 levels are significantly different (two-tailed t-test).

## 5. Discussion

We aimed to understand how the tumor microenvironment impacts tumor progression and metastatic behavior. Most of the efforts in the past focused on defining intrinsic and extrinsic factors involved in tumor progression and metastasis. However, the interpretation of tumor evolution and metastasis has shifted and currently, it is widely accepted that extrinsic factors are actively involved in cancer progression and regression. To answer this question, we used melanoma models to investigate the role of secreted exosomes in tumor microenvironment education and pre-metastatic niche formation. In addition, we explored the influence of bacterial antigens on macrophage polarization in anti-tumor immune effector mechanisms.

In this study, we demonstrated that MSCs, widely abundant in solid tumors as well as in healthy tissues, undergo a marked re-education process upon communication with metastatic cancer cells via exosome-mediated information transfer. This transformation process results in characteristic response patterns corresponding to a given cancerous cell line. We (i) determined the cellular and molecular signals involved in the melanoma-derived exosome-induced, malignant transformation of MSC culture; (ii) described the melanoma-derived exosome-induced tumor progression; (iii) demonstrated the alteration in the expression of PD-1, a melanoma progression marker, and therapeutic target, upon exposure to melanoma-derived exosomes.

Metastasis, a critical phase of melanoma progression, remains a major cause of melanoma mortality and primary challenge in therapy. In this study, we highlighted the emerging roles of melanoma exosomes as coordinators of PMN formation.

Our experimental data provide compelling evidence for the significant tumor regression following the treatment of melanoma lung metastases with the inactivated intracellular pathogen *C. pneumoniae*, and suggest that this microbe may be responsible for tumor regression via the induction of anti-tumoral macrophage polarization. On the other hand, it is generally accepted that anti-tumor immune effector mechanisms overlap with antibacterial immune responses. Macrophages are key players of the immune responses whose M1 type polarization mediates the anti-tumor action of the immune system. In this study, we demonstrated that the heat-inactivated bacterial treatment may induce a complex anti-tumor immune response. The *C. pneumoniae* treatment suppressed metastasis formation (and hence prolonged survival) in immunocompetent, but not in immunodeficient mice. As shown by cytokine/chemokine profiles, the *C. pneumoniae* treatment induced M1-type macrophage polarization and significantly reduced the level of M2-type macrophage in lung metastasis. These data prompted

us to hypothesize that the concomitant anti-microbial immune response may contribute to the anti-tumor effect.

## 6. New Findings

1. Internalized melanoma-derived exosomes conveying oncogenic molecular reprogramming induce the malignant transformation of the recipient MSCs.
2. The melanoma-derived exosomes generate the formation of a melanoma-like, PD-1 overexpressing cell population (mMSC<sup>PD-1+</sup>) from naïve MSCs.
3. Melanoma-derived exosomes and the re-educated melanoma-like MSC<sup>PD-1+</sup> cell population induce tumor progression and facilitate metastatic disease via overexpression of oncogenic factors *in vivo*.
4. Bacterial antigen pattern-induced macrophage polarization and complex anti-tumor immune response indeed leads to the regression of melanoma metastasis.

## Acknowledgement

I would like to express my deep and sincere gratitude to my supervisor and friend, **Krisztina Buzás**, for her excellent scientific guidance, continuous motivation, patience, unconditional trust, and for her unwavering faith. This thesis would not have been possible without her help and support.

I am grateful to the head of the Institute of Biochemistry and the Laboratory of Image Analysis and Machine Learning in the BRC, **Péter Horváth**, for the scientific and infrastructural support of my project.

I am grateful to my colleagues **Mária Harmati, Gabriella Dobra, Lilla Pintér, Mátyás Bukva** for the scientific and technical aid, and for creating a great atmosphere in the laboratory. I would like to thank all help for the other members of the **Laboratory of Image Analysis and Machine Learning**.

I wish to thank **Annamária Marton, Csaba Vizler, Katalin Jósvay** for the scientific and technical support.

I also thank all of the **co-authors** of my publications for their helpful cooperation, and support.

I would like to extend my special thanks to **Péter Závodszky, Péter Gál, Andrea Kocsis, Júlianna Balczerné, József Dobó, István Hajdú, Barbara Végh, László Barna, László Beinrohr**, my colleagues at the Laboratory of Structural Biophysics for their guidance in the complex world of structural biochemistry, their patience, and their support.

The research was supported by GINOP-2.3.2-15-2016-00015; GINOP-2.2.1-15-2017-00052, NKFI-6-K-11493, János Bolyai Research Scholarship of the Hungarian Academy of Sciences, and ÚNKP-19-4.

Lastly, but most importantly, I wish to thank my parents and my brother for their unconditional care, and support throughout my life; my family – who missed me a lot during the last years – for their support, encouragement, and patience.